A two-band model for superconductivity in the checkerboard lattice

2010 J. Phys.: Condens. Matter 22 215701

(http://iopscience.iop.org/0953-8984/22/21/215701)

J. Phys.: Condens. Matter **22** (2010) 215701 (7pp) doi:10.1088/0953-8984/22/21/215701

A two-band model for superconductivity in the checkerboard lattice

E G Santos[1], J R Iglesias[1], C Lacroix[2] and M A Gusmão[1]

[1] Instituto de Física, Universidade Federal do Rio Grande do Sul, CP 15051, 91501-970 Porto Alegre, RS, Brazil
[2] Institut Néel, CNRS, BP 166, 38042 Grenoble Cedex 9, France

Received 11 January 2010, in final form 6 April 2010
Published 30 April 2010
Online at stacks.iop.org/JPhysCM/22/215701

Abstract
Motivated by the superconducting properties of the metallic oxide $Cd_2Re_2O_7$, whose crystal structure is of the pyrochlore type, we propose an electronic model on a *checkerboard lattice*, which can be viewed as a two-dimensional analog of the pyrochlore lattice. Including only charge degrees of freedom, we treat the model via a Bardeen–Cooper–Schrieffer (BCS) approximation, decoupling the interaction terms in real space. Going over to reciprocal space yields a BCS model with two coupled bands. Characteristic properties such as order parameters and specific heat as functions of temperature are obtained. We also discuss the symmetry properties of the superconducting gap in wavevector space and the behavior of the critical temperature as a function of the electronic doping for various values of the interaction strength.

(Some figures in this article are in colour only in the electronic version)

1. Introduction

The pyrochlore lattice, a three-dimensional (3D) network of corner-sharing tetrahedra [1], belongs to a class of structures generally know as *geometrically frustrated lattices* [1–4]. In compounds of the type $A_2B_2O_7$, where A is typically a rare-earth (but can be a metal) and B is a transition metal, both A and B ions occupy the corner sites of pyrochlore sublattices. Extensive experimental studies of such compounds have reported observation of exotic magnetic behavior such as spin liquid or spin ice (for a review see [5]).

$Cd_2Re_2O_7$ was the first compound among pyrochlore oxides that was found to present superconductivity [6–14], with a critical temperature $T_c \approx 1$ K. Other superconducting pyrochlores have been discovered, mostly in the AB_2O_6 family (now A is typically an alkali metal); for example, KOs_2O_6 ($T_c \approx 9.6$ K) [15], $RbOs_2O_6$ ($T_c \approx 6.3$ K) [16, 17], and $CsOs_2O_6$ ($T_c \approx 3.3$ K) [18]. The related spinel compound $LiTi_2O_4$ was already known to be superconducting below 13 K [19, 20]. As often happens, the pairing mechanism is still an open question. In particular, based on the observation of a gap with zeros, Koda *et al* [21] suggested an unconventional superconducting mechanism in KOs_2O_6, driven by spin fluctuations.

From a theoretical point of view, the discovery of superconducting pyrochlores opened new possibilities, as it is interesting to study the nature of superconductivity in a geometrically frustrated lattice. Even though the concept of *frustration* is only meaningful for magnetic interactions, the underlying lattice topology is relevant to electronic band structure, and to interaction patterns in real space that may be involved in superconducting pairing.

In the case of $Cd_2Re_2O_7$, band-structure calculations indicate the presence of a strongly hybridized band, composed of rhenium 5d and oxygen 2p states, with a total width of approximately 3 eV [12, 13]. This relatively large bandwidth may rule out strong-correlation effects [14], suggesting that the superconductivity in $Cd_2Re_2O_7$ is of the conventional type. In agreement with this, measurements of specific heat as a function of temperature find out that the data are consistent with a BCS superconductor [22] in the weak-coupling limit.

Motivated by the above considerations, we present in this work a detailed study of the BCS superconducting solution for a fermion model on the checkerboard lattice, which is usually viewed as a two-dimensional (2D) analog of the pyrochlore lattice. The checkerboard 'dark squares', with next-nearest-neighbor connections along the diagonals, can be viewed as resulting from *flattening* the tetrahedral network in a way that maintains the local connectivity. Spin models on this 2D lattice have been studied in connection with the physics of magnetic frustration in pyrochlores [3, 4]. Fermionic models on this lattice have also been the subject of investigation, mostly with the focus on strongly correlated systems [23–28].

In our approach we decouple the interaction terms in real space [29, 30], starting from a Hamiltonian in Wannier representation. Going then to **k**-space, a two-band BCS model is obtained. Self-consistent equations for the relevant order parameters are determined and solved numerically for varying temperature. We also determine the specific heat behavior with temperature, and construct phase diagrams by plotting T_c as a function of band filling for various coupling values.

The article is organized as follows. In section 2, we present the model Hamiltonian and its treatment within the BCS mean-field scheme, which generates two coupled bands. Section 3 contains our main results for the superconducting gap, specific heat, and phase diagram. Final remarks and conclusions are presented in section 4.

2. Model Hamiltonian

The starting point of our model is a checkerboard structure with identical ions at each site. In $Cd_2Re_2O_7$, these would be Re ions, the only ones with a partially filled shell. For simplicity, we consider that there is a single, non-degenerate orbital per ion, which would be true for a strong local crystal field of sufficiently low symmetry. There are two nonequivalent sites (A and B) per unit cell of the underlying square lattice, defining two interpenetrating sublattices, as illustrated in figure 1.

We use a *tight-binding* formulation, with hopping and intersite interactions between connected sites. The Hamiltonian is written as

$$H = \sum_{i,\delta}\sum_{\alpha,\beta}\sum_{\sigma} t_{\alpha\beta} c^{\dagger}_{i\alpha\sigma} c_{i+\delta,\beta\sigma} + \tfrac{1}{2}\sum_{i,\delta}\sum_{\alpha,\beta}\sum_{\sigma,\sigma'} V_{\alpha\beta} n^{\alpha}_{i\sigma} n^{\beta}_{i+\delta,\sigma'}, \tag{1}$$

with the standard notation for creation, annihilation, and number operators in the Wannier representation. As usual, σ denotes the spin state, α and β are sublattice labels (either A or B), and δ refers to position vectors $\boldsymbol{\delta}$ (not necessarily lattice vectors) relative to site i.

We are not going to discuss the microscopic nature of superconducting coupling, which probably involves electron–phonon interactions in the weak-coupling limit, and could be due to spin fluctuations for strong coupling. We take $V_{\alpha\beta}$ in the second term of equation (1) as an effective (attractive) interaction that allows for superconducting pairing. We consider only intersite attraction since on-site attractive interactions should be prevented by correlations, even if electron–electron interaction is not strong. For symmetry reasons (see figure 1), we can make the choices $t_{AA} = t_{BB} \equiv t$, $t_{AB} = t_{BA} \equiv t'$, $V_{AA} = V_{BB} \equiv -V$, $V_{AB} = V_{BA} \equiv -V'$. With this notation, non-primed symbols refer to the same sublattice (diagonal bonds). Notice that t_{AA} is non-zero only along the direction of **a**, t_{BB} is non-zero only along **b**, while t_{AB} and t_{BA} connect sites of one sublattice with their nearest-neighboring sites on the other one.

3. Noninteracting band structure

Initially, let us analyze only the hopping term. Viewing the Hamiltonian, equation (1), as a sum $H = H_t + H_V$, we rewrite the first term in **k**-space as

$$\begin{aligned} H_t = {} & 2t\sum_{\mathbf{k}\sigma}[\cos(\mathbf{k}\cdot\mathbf{a})c^{\dagger}_{A\mathbf{k}\sigma}c_{A\mathbf{k}\sigma} + \cos(\mathbf{k}\cdot\mathbf{b})c^{\dagger}_{B\mathbf{k}\sigma}c_{B\mathbf{k}\sigma}] \\ & + 4t'\sum_{\mathbf{k}\sigma}\cos(\mathbf{k}\cdot\mathbf{a}/2)\cos(\mathbf{k}\cdot\mathbf{b}/2) \\ & \times [c^{\dagger}_{A\mathbf{k}\sigma}c_{B\mathbf{k}\sigma} + c^{\dagger}_{B\mathbf{k}\sigma}c_{A\mathbf{k}\sigma}]. \end{aligned} \tag{2}$$

Diagonalizing with respect to A and B indexes, gives us the energy bands

$$\varepsilon^{\,a}_{\,b}(\mathbf{k}) = t\left[F_0(\mathbf{k}) \pm \sqrt{F_1^2(\mathbf{k}) + 16\alpha^2 F_2^2(\mathbf{k})}\right], \tag{3}$$

where $\alpha \equiv t'/t$, and we defined

$$\begin{aligned} F_0(\mathbf{k}) &= \cos(\mathbf{k}\cdot\mathbf{a}) + \cos(\mathbf{k}\cdot\mathbf{b}), \\ F_1(\mathbf{k}) &= \cos(\mathbf{k}\cdot\mathbf{a}) - \cos(\mathbf{k}\cdot\mathbf{b}), \\ F_2(\mathbf{k}) &= \cos(\mathbf{k}\cdot\mathbf{a}/2)\cos(\mathbf{k}\cdot\mathbf{b}/2). \end{aligned} \tag{4}$$

These energies and the corresponding densities of states are shown in figure 2 for $\alpha = 0.8$. The narrow low-energy band is a consequence of the lattice geometry. In fact, it becomes completely flat if we choose $\alpha = 1$. Despite the simplicity of our model, the main qualitative features of the energy spectrum are consistent with those obtained through band-structure calculations [13] for $Cd_2Re_2O_7$. On the other hand, the van Hove singularities seen in the right panel of figure 2 are a two-dimension artifact, and their possible physical effects have no counterpart in the pyrochlore lattice.

We can write the hopping Hamiltonian, equation (2), in its diagonal form,

$$H_t = \sum_{\mathbf{k}}[\varepsilon_a(\mathbf{k})n^a_{\mathbf{k}\sigma} + \varepsilon_b(\mathbf{k})n^b_{\mathbf{k}\sigma}], \tag{5}$$

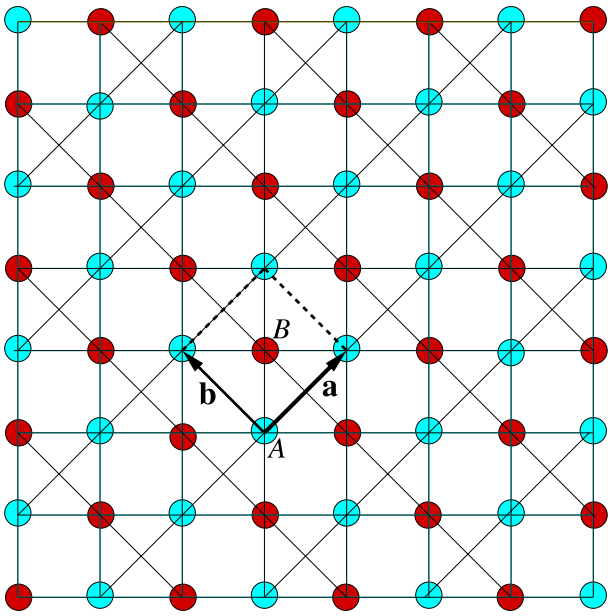

Figure 1. Possible choice of site labeling on the checkerboard structure, showing a pair of primitive vectors that define a square lattice unit cell.

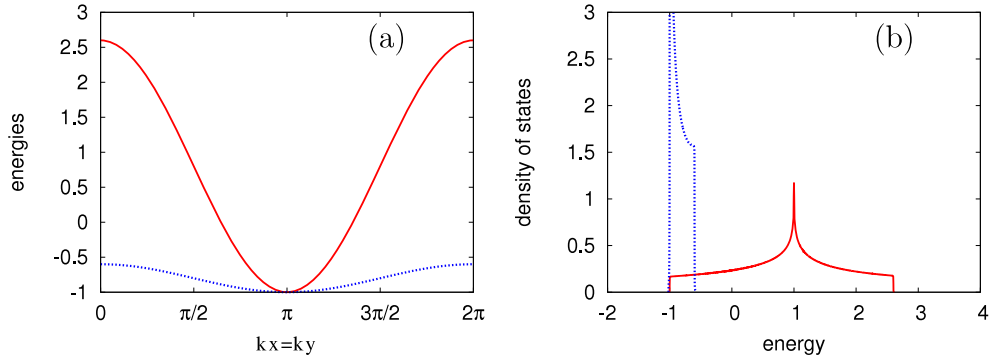

Figure 2. (a) Energy bands in the absence of interactions along the line $k_x = k_y$. The wide and narrow bands are, respectively, a and b (see equation (3)) for $\alpha = 0.8$. (b) Densities of states. We chose $2t$ as the energy unit and $1/a$ as the wavevector unit, where $a \equiv |\mathbf{a}| = |\mathbf{b}|$.

where the number operators are written in terms of new creation and annihilation operators for electrons in the a and b bands. The relations between these new operators and the original ones are

$$\begin{aligned} a_{\mathbf{k}\sigma} &\equiv \frac{1}{r_{\mathbf{k}}}(c_{A\mathbf{k}\sigma} + \phi_{\mathbf{k}} c_{B\mathbf{k}\sigma}), \\ b_{\mathbf{k}\sigma} &\equiv \frac{1}{r_{\mathbf{k}}}(c_{B\mathbf{k}\sigma} - \phi_{\mathbf{k}} c_{A\mathbf{k}\sigma}), \end{aligned} \tag{6}$$

where

$$\phi_{\mathbf{k}} \equiv \frac{\varepsilon_a(\mathbf{k})/2t - \cos(\mathbf{k}.\mathbf{a})}{2\alpha F_2(\mathbf{k})}, \qquad r_{\mathbf{k}} = \sqrt{1+\phi_{\mathbf{k}}^2}. \tag{7}$$

4. Interaction terms—BCS decoupling

We focus now on the interaction term of equation (1),

$$H_V = \tfrac{1}{2}\sum_{\sigma\sigma'}\sum_{\alpha\beta}\sum_{i\delta} V_{\alpha\beta}\, n^{\alpha}_{i\sigma} n^{\beta}_{i+\delta,\sigma'}, \tag{8}$$

with $V_{\alpha\beta}$ assuming either the value $-V$ or $-V'$, for intra- and inter-sublattice interactions respectively, with $V, V' > 0$, as introduced in section 2.

Explicitly writing the number operators that appear in equation (8) in terms of creation and annihilation operators, and performing the usual BCS decoupling, we have

$$\begin{aligned} c^{\dagger}_{\alpha i\sigma} c_{\alpha i\sigma} c^{\dagger}_{\beta,i+\delta,\sigma'} c_{\beta,i+\delta,\sigma'} &\simeq \langle c^{\dagger}_{\alpha i\sigma} c^{\dagger}_{\beta,i+\delta,\sigma'}\rangle c_{\beta,i+\delta,\sigma'} c_{\alpha i\sigma} \\ &+ \langle c_{\beta,i+\delta,\sigma'} c_{\alpha i\sigma}\rangle c^{\dagger}_{\alpha i\sigma} c^{\dagger}_{\beta,i+\delta,\sigma'} \\ &- \langle c^{\dagger}_{\alpha i\sigma} c^{\dagger}_{\beta,i+\delta,\sigma'}\rangle\langle c_{\beta,i+\delta,\sigma'} c_{\alpha i\sigma}\rangle. \end{aligned} \tag{9}$$

We now define

$$\Delta_{\alpha\beta} \equiv -V_{\alpha\beta}\langle c_{\beta,i+\delta,\sigma'} c_{\alpha i\sigma}\rangle. \tag{10}$$

With the above notation, we approximate the product of number operators in equation (8) as

$$n^{\alpha}_{i\sigma} n^{\beta}_{i+\delta,\sigma'} \simeq \{[\Delta_{\alpha\beta}\, c^{\dagger}_{\alpha i\sigma} c^{\dagger}_{\beta,i+\delta,\bar{\sigma}} + \text{h.c.}] - |\Delta_{\alpha\beta}|^2\}\delta_{\sigma'\bar{\sigma}}, \tag{11}$$

where h.c. represents the Hermitian conjugate of the previous term, and we are restricting our analysis to singlet pairing ($\bar{\sigma} \equiv -\sigma$).

Similarly to what we did with the hoppings in section 2, we choose $\Delta_{AA} = \Delta_{BB} \equiv \Delta$ and $\Delta_{AB} = \Delta_{BA} \equiv \Delta'$. This is not the most general choice, as one could allow for different signs of the gap parameters along orthogonal directions in the lattice, with consequences to the gap symmetry in $\mathbf{k}$-space, as we will discuss later. With these choices, the interaction Hamiltonian becomes

$$\begin{aligned} H^{\text{BCS}}_{\text{int}} = &-\sum_{i\alpha}\sum_{\delta}(\Delta\, c^{\dagger}_{\alpha i\uparrow} c^{\dagger}_{\alpha,i+\delta,\downarrow} + \text{h.c.}) \\ &- \sum_{i}\sum_{\substack{\alpha,\beta \\ \alpha\neq\beta}}\sum_{\delta}(\Delta'\, c^{\dagger}_{\alpha i\uparrow} c^{\dagger}_{\beta,i+\delta,\downarrow} + \text{h.c.}) + \bar{E}_0, \end{aligned} \tag{12}$$

where

$$\bar{E}_0 \equiv 2N\left(\frac{|\Delta|^2}{V} + \frac{|\Delta'|^2}{V'}\right). \tag{13}$$

Fourier transforming to $\mathbf{k}$-space, we obtain

$$\begin{aligned} H^{\text{BCS}}_{\text{int}} = &-2\sum_{\mathbf{k}}\{\Delta[\cos(\mathbf{k}\cdot\mathbf{a}) c^{\dagger}_{A,\mathbf{k}\uparrow} c^{\dagger}_{A,-\mathbf{k}\downarrow} \\ &+ \cos(\mathbf{k}\cdot\mathbf{b}) c^{\dagger}_{B,\mathbf{k}\uparrow} c^{\dagger}_{B,-\mathbf{k}\downarrow}] + 2\Delta'\cos(\mathbf{k}\cdot\mathbf{a}/2)\cos(\mathbf{k}\cdot\mathbf{b}/2) \\ &\times [c^{\dagger}_{A,\mathbf{k}\uparrow} c^{\dagger}_{B,-\mathbf{k}\downarrow} + c^{\dagger}_{B,\mathbf{k}\uparrow} c^{\dagger}_{A,-\mathbf{k}\downarrow}] + \text{h.c.}\} + \bar{E}_0. \end{aligned} \tag{14}$$

Finally, using equations (6) to rewrite the interaction part in terms of the a and b band operators, adding the hopping term, equation (5), and adopting the usual simplified notation $\mathbf{k}\uparrow \equiv \mathbf{k}$ and $-\mathbf{k}\downarrow \equiv -\mathbf{k}$, we can write the full Hamiltonian as a two-band BCS model of the form

$$\begin{aligned} H = &\sum_{\mathbf{k}}[\varepsilon_a(\mathbf{k})(a^{\dagger}_{\mathbf{k}} a_{\mathbf{k}} + a^{\dagger}_{-\mathbf{k}} a_{-\mathbf{k}}) - \Delta^{aa}_{\mathbf{k}} a^{\dagger}_{\mathbf{k}} a^{\dagger}_{-\mathbf{k}} - (\Delta^{aa}_{\mathbf{k}})^* a_{-\mathbf{k}} a_{\mathbf{k}}] \\ &+ \sum_{\mathbf{k}}[\varepsilon_b(\mathbf{k})(b^{\dagger}_{\mathbf{k}} b_{\mathbf{k}} + b^{\dagger}_{-\mathbf{k}} b_{-\mathbf{k}}) - \Delta^{bb}_{\mathbf{k}} b^{\dagger}_{\mathbf{k}} b^{\dagger}_{-\mathbf{k}} - (\Delta^{bb}_{\mathbf{k}})^* b_{-\mathbf{k}} b_{\mathbf{k}}] \\ &- \sum_{\mathbf{k}}[\Delta^{ab}_{\mathbf{k}}(a^{\dagger}_{\mathbf{k}} b^{\dagger}_{-\mathbf{k}} + b^{\dagger}_{\mathbf{k}} a^{\dagger}_{-\mathbf{k}}) \\ &+ (\Delta^{ab}_{\mathbf{k}})^*(b_{-\mathbf{k}} a_{\mathbf{k}} + a_{-\mathbf{k}} b_{\mathbf{k}})] + \bar{E}_0. \end{aligned} \tag{15}$$

The gap functions $\Delta^{aa}_{\mathbf{k}}$, $\Delta^{bb}_{\mathbf{k}}$, and $\Delta^{ab}_{\mathbf{k}}$ are written as

$$\begin{aligned} \Delta^{aa}_{\mathbf{k}} &= [2\Delta\, F_a(\mathbf{k}) + 8\Delta'\,\phi_{\mathbf{k}} F_2(\mathbf{k})]/r^2_{\mathbf{k}}, \\ \Delta^{bb}_{\mathbf{k}} &= [2\Delta\, F_b(\mathbf{k}) - 8\Delta'\,\phi_{\mathbf{k}} F_2(\mathbf{k})]/r^2_{\mathbf{k}}, \\ \Delta^{ab}_{\mathbf{k}} &= [4\Delta'(1-\phi^2_{\mathbf{k}}) F_2(\mathbf{k}) - 2\Delta\,\phi_{\mathbf{k}} F_1(\mathbf{k})]/r^2_{\mathbf{k}}, \end{aligned} \tag{16}$$

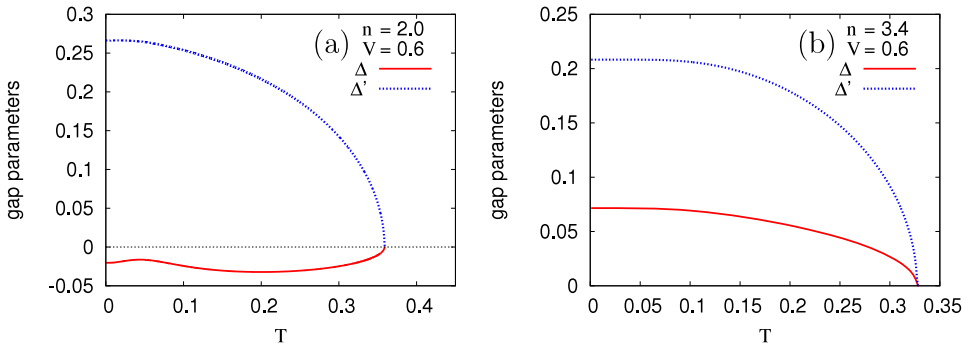

Figure 3. Variation of the gap parameters with temperature for the stoichiometric case $n = 2.0$ (a), and a typical case at high filling, $n = 3.4$ (b), with an arbitrary choice of $V = V' = 0.6$ (in units of $2t$).

in terms of the previously defined $F_0(\mathbf{k})$, $F_1(\mathbf{k})$, $F_2(\mathbf{k})$, $\phi_\mathbf{k}$, $r_\mathbf{k}$ (see equations (4) and (7)), and two additional definitions:

$$F_a(\mathbf{k}) = \cos(\mathbf{k}\cdot\mathbf{a}) + \phi_\mathbf{k}^2\cos(\mathbf{k}\cdot\mathbf{b}),$$
$$F_b(\mathbf{k}) = \cos(\mathbf{k}\cdot\mathbf{b}) + \phi_\mathbf{k}^2\cos(\mathbf{k}\cdot\mathbf{a}). \tag{17}$$

Two-band BCS models have been studied by several authors (see, for example, [31–35]). Here, we explore the specific aspects of our model, associated with the lattice topology.

4.1. Superconducting solution

Continuing with the usual procedure, we can write the Hamiltonian (15) in its diagonal form,

$$H = \sum_\mathbf{k}[E_1(\mathbf{k})(\alpha_{1\mathbf{k}}^\dagger\alpha_{1\mathbf{k}} + \beta_{1\mathbf{k}}^\dagger\beta_{1\mathbf{k}}) + E_2(\mathbf{k})(\alpha_{2\mathbf{k}}^\dagger\alpha_{2\mathbf{k}} + \beta_{2\mathbf{k}}^\dagger\beta_{2\mathbf{k}})] + \bar{E}, \tag{18}$$

where we define

$$\bar{E} = \sum_\mathbf{k}[\bar{\varepsilon}_a(\mathbf{k}) + \bar{\varepsilon}_b(\mathbf{k}) - E_1(\mathbf{k}) - E_2(\mathbf{k})] + \bar{E}_0. \tag{19}$$

The energy eigenvalues $E_1(\mathbf{k})$ and $E_2(\mathbf{k})$ are given by

$$E_{\frac{1}{2}}^2(\mathbf{k}) = \tfrac{1}{2}[E_a^2(\mathbf{k}) + E_b^2(\mathbf{k}) + 2|\Delta_\mathbf{k}^{ab}|^2 \mp \sqrt{R_\mathbf{k}^{ab}}], \tag{20}$$

where

$$E_a^2(\mathbf{k}) = \bar{\varepsilon}_a^2(\mathbf{k}) + |\Delta_\mathbf{k}^{aa}|^2, \qquad E_b^2(\mathbf{k}) = \bar{\varepsilon}_b^2(\mathbf{k}) + |\Delta_\mathbf{k}^{bb}|^2, \tag{21}$$

$$R_\mathbf{k}^{ab} = [E_a^2(\mathbf{k}) - E_b^2(\mathbf{k})]^2 + 4|\Delta_\mathbf{k}^{ab}|^2 \times [E_a^2(\mathbf{k}) + E_b^2(\mathbf{k}) - 2\bar{\varepsilon}_a(\mathbf{k})\bar{\varepsilon}_b(\mathbf{k})] + 4(\Delta_\mathbf{k}^{aa})^*(\Delta_\mathbf{k}^{bb})^*(\Delta_\mathbf{k}^{ab})^2 + 4\Delta_\mathbf{k}^{aa}\Delta_\mathbf{k}^{bb}[(\Delta_\mathbf{k}^{ab})^*]^2. \tag{22}$$

We are actually working now with $H - \mu N_\mathrm{e}$, μ being the chemical potential and N_e the total number of electrons. For this reason the bare band energies have been replaced by $\bar{\varepsilon}_a(\mathbf{k}) \equiv \varepsilon_a(\mathbf{k}) - \mu$ and $\bar{\varepsilon}_b(\mathbf{k}) \equiv \varepsilon_b(\mathbf{k}) - \mu$, and μ must be fixed through the condition

$$2\frac{1}{N}\sum_\mathbf{k}[f(\bar{\varepsilon}_a(\mathbf{k})) + f(\bar{\varepsilon}_b(\mathbf{k}))] = n, \tag{23}$$

where $n \equiv N_\mathrm{e}/N$ is the number of electrons per unit cell.

The operators $\alpha_{1\mathbf{k}}$, $\beta_{1\mathbf{k}}$, $\alpha_{2\mathbf{k}}$, $\beta_{2\mathbf{k}}$ in equation (18) are linear combinations of the operators $a_\mathbf{k}^\dagger$, $a_{-\mathbf{k}}$, $b_\mathbf{k}^\dagger$, and $b_{-\mathbf{k}}$. These new operators describe free-fermion excitations out of the superconducting ground-state. We can thus write the internal energy and the free energy of the system as

$$U = 2\sum_{\lambda\mathbf{k}} E_\lambda(\mathbf{k})\, f(E_\lambda(\mathbf{k})) + \bar{E} + \mu N_\mathrm{e}, \tag{24}$$

$$F = 2k_\mathrm{B}T\sum_{\lambda\mathbf{k}} \ln[1 - f(E_\lambda(\mathbf{k}))] + \bar{E} + \mu N_\mathrm{e}, \tag{25}$$

where $f(E)$ is the Fermi–Dirac distribution, and $\lambda = 1, 2$.

Self-consistent equations for the order parameters Δ and Δ' can then be obtained by minimizing the free energy with respect to these parameters. We adopt the simplifying assumption that Δ and Δ' are real. Then, the resulting equations are

$$\Delta = \frac{V}{4}\sum_\mathbf{k}\left[\tanh\left(\frac{E_1(\mathbf{k})}{2T}\right)\frac{\partial E_1(\mathbf{k})}{\partial\Delta} + \tanh\left(\frac{E_2(\mathbf{k})}{2T}\right)\frac{\partial E_2(\mathbf{k})}{\partial\Delta}\right],$$
$$\Delta' = \frac{V'}{4}\sum_\mathbf{k}\left[\tanh\left(\frac{E_1(\mathbf{k})}{2T}\right)\frac{\partial E_1(\mathbf{k})}{\partial\Delta'} + \tanh\left(\frac{E_2(\mathbf{k})}{2T}\right)\frac{\partial E_2(\mathbf{k})}{\partial\Delta'}\right]. \tag{26}$$

Once these equations are (numerically) solved for different temperatures we can determine the critical temperature T_c, and calculate the specific heat from the thermal derivative of the internal energy U.

5. Results

We start by analyzing the variation of the order parameters Δ and Δ' with temperature in two representative situations: low and high band filling. Keeping in mind our experimental motivation, $Cd_2Re_2O_7$ has basically two compensated overlapping bands, with the Fermi level located near the top of a narrow hole-like band, as discussed in section 3. This corresponds to $n = 2$ and implies that $\alpha < 1$ in our checkerboard lattice model, so that we will keep our choice of $\alpha = 0.8$ in all calculations. Figure 3(a) shows the gap

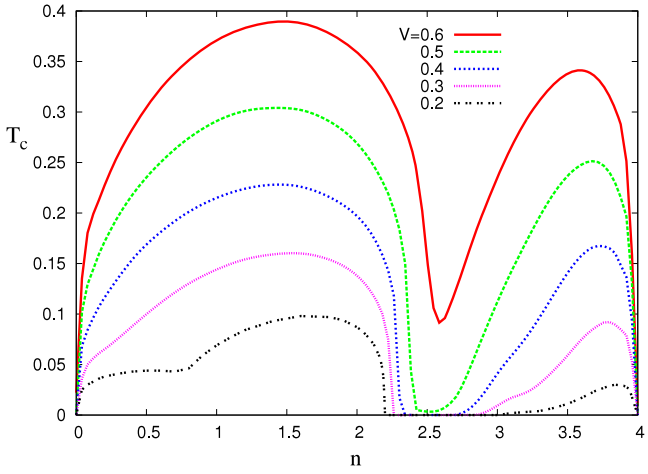

Figure 4. Critical superconducting temperature as a function of band filling for some values of the coupling $V(=V')$ (in units of $2t$).

parameters for this situation. Notice the sign reversal of Δ with respect to Δ', which should be interpreted as a phase difference, since we are treating these parameters as real. This sign difference disappears at high band fillings, as exemplified in figure 3(b). However, there is a wide range of fillings below $n = 2$ where a sign reversal of Δ occurs (either smoothly or discontinuously) at some finite temperature $T^* < T_c$.

Slightly above $n = 2$, near the electron concentration for which the narrow b-band becomes completely filled, superconductivity tends to be suppressed, but T_c rises again at higher fillings. For a better visualization of these regimes, figure 4 shows phase diagrams T_c versus n for different values of the coupling V. The results presented here are only for $V' = V$. However, we should mention that the overall scale of the phase diagram is set by V', with little change due to variations of V.

Figure 4 shows clearly the existence of different regimes for low and high electron concentrations. For sufficiently weak-coupling, each of these regimes is limited by a quantum critical point, where T_c goes to zero at a non-trivial band filling, i.e. not empty or completely filled band. Given the scale of temperatures in the phase diagram, the experimentally relevant situation should correspond to V even smaller, which means that the superconducting transition in $Cd_2Re_2O_7$, for which $T_c \sim 1$ K, could occur near a quantum critical point.

The different regimes discussed above can also be observed in the thermal behavior of the specific heat, as shown in figure 5. Notice that the large-n case shows the usual behavior in the presence of an excitation gap for $T \to 0$. In contrast, for $n = 2$ one sees no indication of a true gap.

These results indicate that we should see nodes in the zero-temperature superconducting gap as a function of wavevector. The actual gap is the minimum value of the lowest energy $E_1(\mathbf{k})$. A three-dimensional plot of this energy, for $n = 2$ and $T \to 0$, is shown in figure 6. One can see that it approaches zero at places near the zone corners where the a-band branch of the Fermi surface (FS) is located. A better visualization of the gap zeros is provided by figure 7(a). For large n, as exemplified in figure 7(b) for a different coupling, the gap is modulated in $\mathbf{k}$-space along the Fermi surface, but is always finite. We can classify these symmetries as s $-$ s and s $+$ s, respectively, since we have extended s-wave symmetry associated to both Δ and Δ', with opposite phases in one case and the same phase in the other. The symmetry change occurs across the region around $n = 2.5$ where superconductivity is suppressed (see figure 4). It is worth mentioning that the s $-$ s phase was also found by Huang *et al* [28] in the strongly correlated limit (holes in the t–J model), for the same region of t'/t (our notation has t and t' exchanged with respect to that of [28]).

Figures 6 and 7 help clarify the scenario already shown by figure 4. For low band filling, up to slightly above $n = 2$, there are FS branches on both bands, but the low-energy physics in the superconducting state is only connected to the a-band FS, where the gap is small, and can even have zeros. Notice in figure 6 that the excitation energy is very large near the zone center, where the b-band FS is located. For larger n, the excitation energies continue to be smaller near the only remaining FS, that of band a, which eventually moves over to the zone center, turning from electron-like to hole-like.

6. Conclusions

In this work, we developed a detailed study of superconductivity in an electronic model on the *checkerboard* structure, intended to mimic the pyrochlore lattice in two dimensions. The tight-binding density of states indeed shows some similarities with band-structure calculations for $Cd_2Re_2O_7$, the superconducting pyrochlore compound that motivates our

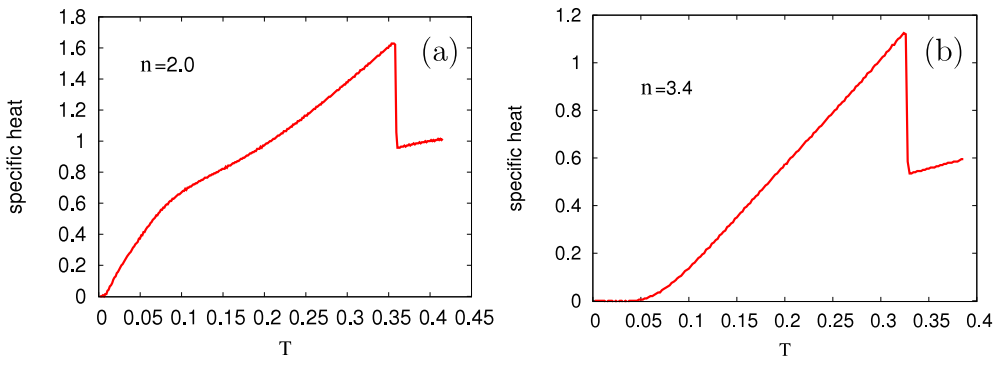

Figure 5. Specific heat versus temperature for $n = 2.00$ (a) and $n = 3.4$ (b), with $V = V' = 0.6$ (in units of $2t$).

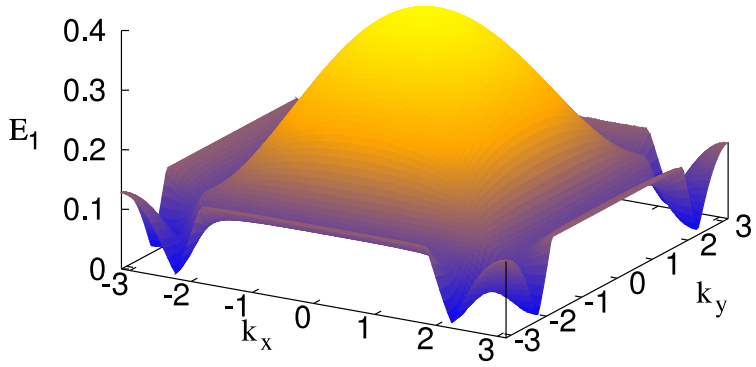

Figure 6. Surface plot of the lowest energy, $E_1(\mathbf{k})$, for $n = 2.00$, $T \to 0$, and with $V = V' = 0.6$. The energy gap goes to zero at the sharp minima near the zone corners.

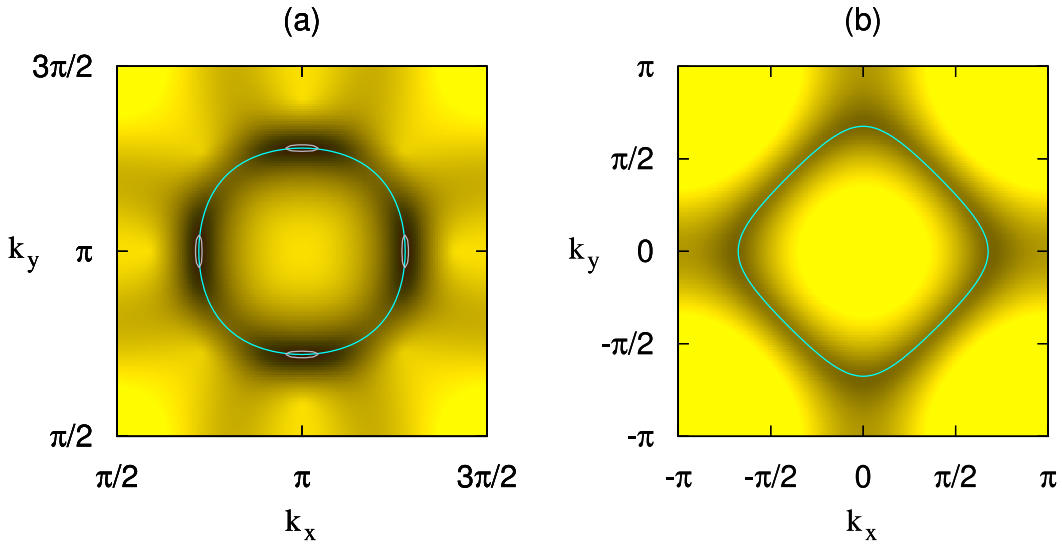

Figure 7. Map plots of $E_1(\mathbf{k})$ for $n = 2$, $V = V' = 0.6$ (a), and $n = 3.4$, $V = V' = 0.4$ (b). Darker regions correspond to lower energy values. A closed line shows the normal-state a-band Fermi surface in each case. The small ellipses in (a) are nearly zero contours of $E_1(\mathbf{k})$, identifying the points where the gap vanishes.

investigation. With an effective electron–electron interaction between neighboring sites, we performed a BCS decoupling and obtained a two-band BCS model. The superconducting solutions showed a variety of regimes as the band filling or coupling are changed, with s − s symmetry at low filling, s + s symmetry at high n, and a suppression of superconductivity in between, giving rise to the appearance of quantum critical points.

We do not claim that all these features are relevant to the superconductivity observed in $Cd_2Re_2O_7$, since two-dimensional features intrinsic to our model may play an important role. But it could be interesting to perform experimental investigations on doped samples to check the behavior of T_c as a function of electron concentration. On the other hand, the model in itself is very rich, and can be further explored. For instance, one can easily allow for mixtures of d- and s-wave symmetries. It would also be interesting to take into account spin correlations, which we have neglected here, studying their interplay with superconductivity in the presence of magnetic frustration.

Acknowledgments

We acknowledge support from Brazilian agencies, Conselho Nacional de Desenvolvimento Científico e Tecnológico (CNPq) and the Coordenação de Aperfeiçoamento de Pessoal de Nível Superior (CAPES).

References

[1] Pinettes C, Canals B and Lacroix C 2002 *Phys. Rev.* B **66** 024422
[2] Canals B and Lacroix C 2000 *Phys. Rev.* B **61** 1149
[3] Canals B 2002 *Phys. Rev.* B **65** 184408
[4] Elhajal M, Canals B and Lacroix C 2001 *J. Magn. Magn. Mater.* **226** 379
[5] Gardner J S, Gingras M and Greedan J E 2010 *Rev. Mod. Phys.* **82** 53
[6] Sakai H, Yoshimura K, Ohno H, Kato H, Kambe S, Waltedt R E, Matsuda T D, Haga Y and Onuki Y 2001 *J. Phys.: Condens. Matter* **13** L785
[7] Jin R, He J, McCall S, Alexander C, Drymiotis F and Mandrus D 2001 *Phys. Rev.* B **64** 180503

[8] Hanawa M, Muraoka Y, Tayama T, Sakakibara T, Yamaura J and Hiroi Z 2001 *Phys. Rev. Lett.* **87** 187001
[9] Hiroi Z and Hanawa M 2002 *J. Phys. Chem. Solids* **63** 1021
[10] Vyaselev O, Kobayash K, Arai K, Yamazaki J, Kodama K, Takigawa M, Hanawa M and Hiroi Z 2002 *J. Phys. Chem. Solids* **63** 1031
[11] Vyaselev O, Arai K, Kobayashi K, Kodama K, Takigawa M, Hanawa M and Hiroi Z 2002 *Phys. Rev. Lett.* **89** 017001
[12] Harina H 2002 *J. Phys. Chem. Solids* **63** 1035
[13] Sing D J, Blaha P, Schwarz K and Sofo J O 2002 *Phys. Rev.* B **65** 155109
[14] Hiroi Z, Yamaura J-I, Yonezawa S and Harima H 2007 *Physica* C **460–462** 20
[15] Yonezawa S, Muraoka Y, Matsushita Y and Hiroi Z 2004 *J. Phys.: Condens. Matter* **16** L9
[16] Brühwiler M, Kazakov S M, Zhigadlo N D, Karpinski J and Batlogg B 2004 *Phys. Rev.* B **70** 020503R
[17] Yonezawa S, Muraoka Y, Matsushita Y and Hiroi Z 2004 *J. Phys. Soc. Japan* **73** 819
[18] Yonezawa S, Muraoka Y and Hiroi Z 2004 *J. Phys. Soc. Japan* **73** 1655
[19] Johnston D C, Prakash H, Zachariasen W H and Viswanathan R 1973 *Mater. Res. Bull.* **8** 777
[20] Johnston D C 1976 *J. Low Temp. Phys.* **25** 145
[21] Koda A, Higemoto W, Ohishi K, Saha S R, Kadono R, Yonezawa S, Muraoka Y and Hiroi Z 2005 *J. Phys. Soc. Japan* **74** 1678
[22] Bardeen J, Cooper L N and Schrieffer J R 1957 *Phys. Rev.* **108** 1175
[23] Yoshioka T, Koga A and Kawakami N 2006 *Physica* B **378–380** 294
[24] Pollmann F, Betouras J J, Shtengel K and Fulde P 2006 *Phys. Rev. Lett.* **97** 170407
[25] Chen C 2002 *Phys. Lett.* A **303** 81
[26] Pollmann F, Betouras J J, Runge E and Fulde P 2007 *J. Magn. Magn. Mater.* **310** 966
[27] Poilblanc D, Penc K and Shannon N 2007 *Phys. Rev.* B **75** 220503R
[28] Huang H-X, Li Y-Q, Gan J-Y, Chen Y and Zhang F-C 2007 *Phys. Rev.* B **75** 184523
[29] Arrachea L and Aligia A A 1997 *Physica* C **289** 70
[30] Arrachea L and Aligia A A 1999 *Phys. Rev.* B **59** 1333
[31] Suhl H, Matthias B T and Walker L R 1959 *Phys. Rev. Lett.* **3** 552
[32] Lagos R E and Cabrera G G 2003 *Braz. J. Phys.* **33** 713
[33] Entin-Wohlman O and Imry Y 1989 *J. Phys.: Condens. Matter* **1** 9045
[34] Konsin P and Sorkin B 2004 *Supercond. Sci. Technol.* **17** 1472
[35] Marsiglio F and Hirsch J E 2008 *Physica* C **468** 1047